

Visualization of the self-assembly of silica nanochannels reveals growth mechanism

Christophe Jung, Peter Schwaderer, Mark Dethlefsen, Ralf Köhn, Jens Michaelis* and Christoph Bräuchle*

Self-assembled mesoporous structures with well-ordered nanoscale channels could be used in applications such as molecular separation, nano-optics, molecular electronics, nanomedicine and catalysis^{1–7}. However, the domain sizes that can be created in such systems are limited by our lack of a detailed understanding of the relevant growth processes^{8–12}. Here we report the real-time observation of domain growth in the self-assembly of silica nanochannels using fluorescence polarization imaging and atomic force microscopy. We show that transient lamellar structures precede the formation of hexagonal layers, and that the layer growth follows two distinct pathways. In addition, the domains are grown on a mesoporous film substrate, which acts as a sieve and allows control of the delivery of the reactive species. We use these insights and capabilities to grow layers of well-ordered silica nanochannels with domain sizes of up to ~ 0.3 μm .

Layers containing arrays of well-ordered silica nanochannels can be produced through the self-assembly of surfactant molecules and polymerizable silica species^{9,13–15}. Within these layers are randomly organized small domains (up to a few $100 \times 100 \text{ nm}^2$), inside of which nanochannels with uniform cross-sections are hexagonally arranged. The orientation of the channels and the domain structure can be determined by investigating the dynamics of single dye molecules incorporated as guests^{16–18}.

For many applications of these materials (for example, in molecular separation), there is a requirement for ultralarge domains of highly oriented hexagonal mesoporous systems in the millimetre range. Over recent years, extensive effort has been expended in preparing mesoporous materials with a greater degree of order in the channel system^{18–23}. However, the formation of highly ordered mesoporous domains with dimensions in the range of tens of micrometres and above is subject to serious nanotechnological challenges, because formation and growth mechanisms are not, as yet, well understood. To overcome these limitations it is therefore important to develop technologies that lead to an understanding of the growth process and provide means for its control.

Here, we report the *in situ* visualization of the formation and growth of large domains of thin mesoporous layers self-assembling on top of a flat substrate. The fabrication technique uses the substrate itself as a material reservoir, which supplies the ingredients for the formation of the nanostructures (Fig. 1a, left panel). The substrate is a thin mesostructured cetyltrimethylammonium bromide (CTAB)/silica film prepared from the precursor materials by spin-coating⁹. It is important to note that the substrate still contains freely diffusing reactive molecules such as silica precursors and surfactant molecules. In addition to lateral diffusion inside the pores, they can reach the surface of the film through defects such as domain boundaries, thus allowing for control of the reactive

species needed for domain growth. The silica channel system is templated by a hexagonal arrangement of cylindrical micelles of the surfactant CTAB, leading to pore–pore distances of 3–4 nm. This reaction mixture leads to the spontaneous formation of ultralarge domains of thin mesoporous layers (as schematically illustrated in Fig. 1a, right panel). The formation kinetics and domain size can be controlled by adjusting the temperature and relative humidity (see Methods for experimental details).

Tapping-mode atomic force microscopy (AFM) was used to investigate the topography of the thin mesoporous layers grown on a substrate with a thickness of ~ 120 nm (Fig. 1b)²⁴. The observed hexagonal structure is extremely flat, with dimensions of $\sim 30 \mu\text{m} \times 50 \mu\text{m}$, except near the centre where additional discrete layers are observed. The height profile of this domain (determined by a cross-section of the AFM data, Fig. 1c) indicates the existence of discrete nanochannel layers. This is further confirmed by a histogram of the height data, which shows seven well-separated peaks (Supplementary Fig. S1). The determined thickness of the first layer is 6.7 ± 0.4 nm. As the layer-to-layer distance for the hexagonal phase of a mesostructured CTAB/silica film is in the range of 3–4 nm (as determined by X-ray diffractometry)¹⁹ we conclude that the first large plateau of the AFM image corresponds to two layers of cylindrical micelles of CTAB embedded in a polymerized silica matrix (see Supplementary Figs S3 and S4 for details and additional experimental evidence). Up to five discrete mesoporous monolayers with identical thicknesses of 3.0 ± 0.4 nm are observed on top of the bilayer. Although domain sizes and shapes varied between samples, a mesoporous bilayer was always encountered first, followed by a varying number of successive monolayers. Domain formation therefore requires a hexagonally packed bilayer, because a single monolayer is not stable. Each additional layer is then stabilized by the underlying layer.

To prove that the observed topographical structures are ordered domains of hexagonally arranged channels it is important to determine the orientation of the channel system within such a domain. Terrylenediimide molecules (TDI, structure shown in Fig. 1a, right panel)²⁵ incorporated as guest in the channels of the mesoporous material constitute excellent probes with which to investigate pore orientation¹⁸. Inside the channels, the guest molecules cannot rotate around their long axis, because the effective diameter of the template-filled pores ($< 2\text{--}3$ nm) is smaller than the length of the TDI molecule (3.2 nm). The orientation of the channel system in the hexagonal domains can therefore be deduced from the orientation of the TDI molecules, which are perfectly aligned along the CTAB-filled pores. The dye orientation was determined using polarization fluorescence microscopy (Fig. 1d, see also Methods and Supplementary Fig. S2)^{18,19}. A combined image was then obtained by overlaying the extracted orientation onto the topography as

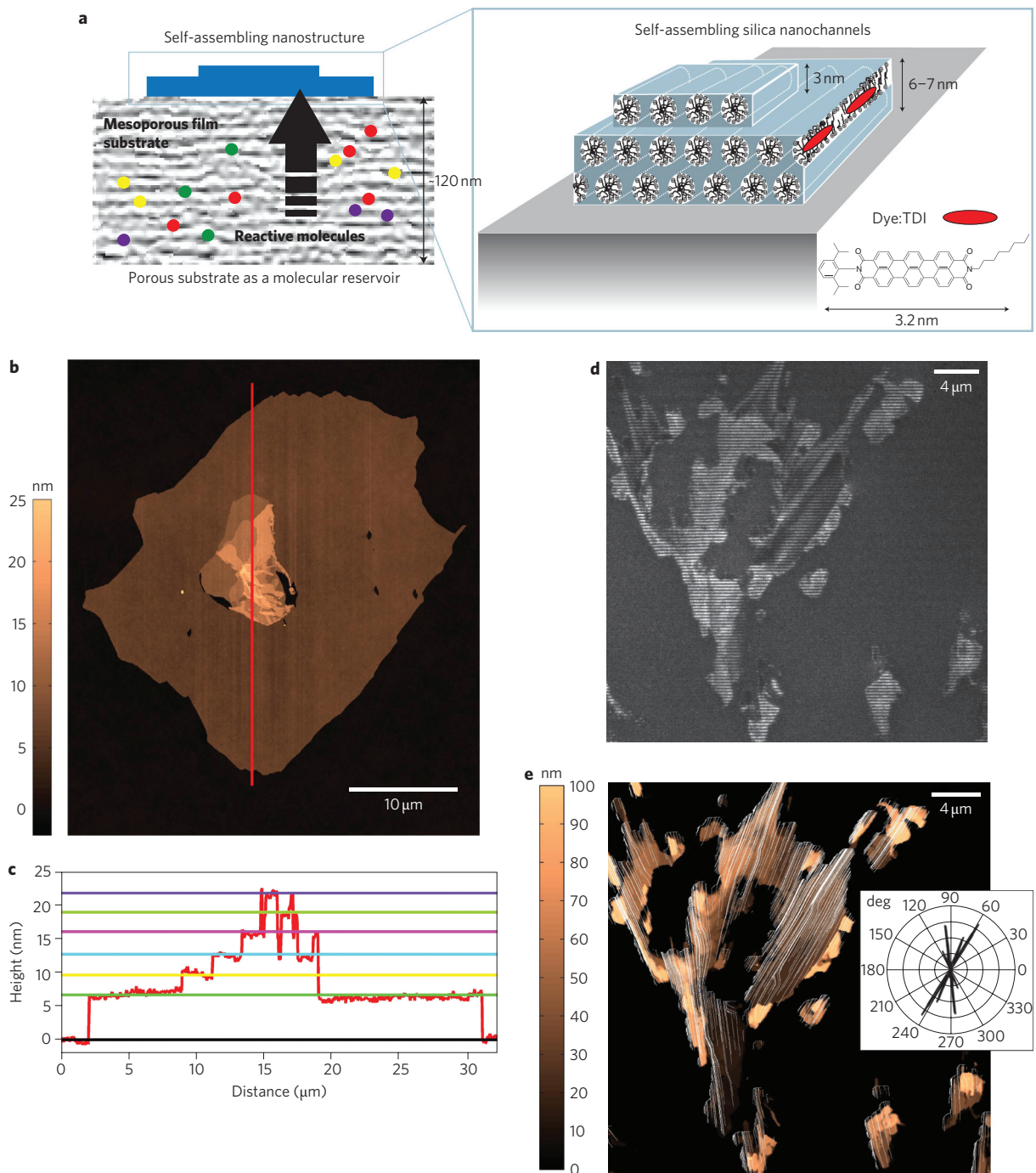


Figure 1 | Silica mesoporous layers. **a**, Sketch of mesoporous layers grown on top of a mesoporous film substrate. Left panel: illustration of how reactive material (shown as coloured circles) is delivered to the surface of the mesoporous film substrate (in grey) by diffusion through defects. Right panel: hexagonally ordered thin mesoporous layers formed on top of the substrate, including CTAB molecules and the TDI dye (in red), which is aligned along the channels. **b**, AFM image of a domain of mesoporous layers exhibiting up to seven layers. For visualization and automated analysis of plateau height and size, the original data were modified using different filter algorithms (Supplementary Fig. S8). **c**, Height profile of the cross-section along the red line in **b**. The surface of the underlying mesoporous film substrate is set to zero. **d**, Polarization-modulated confocal images. The striped pattern of the fluorescence signal arising from the TDI molecules incorporated as guests in the nanochannels indicates that the fluorophores are strongly oriented. **e**, AFM image of the area identical to that of **d**, showing a complex multilayer structure. The pore direction of the mesoporous layers is overlaid as white lines. The direction of the channel was deduced from the orientation of the TDI molecules obtained from image analysis of **d** (for details see Supplementary Fig. S2). Inset: histogram of the orientations displayed as a polar plot in which the frequency of observation of the orientations is encoded in the length of the lobes.

determined by AFM (Fig. 1e). The orientations are additionally displayed as a polar plot (inset) in which the frequency of observation of the orientations is encoded in the length of the lobes. The nanochannels are linear over several micrometres, demonstrating the high degree of order.

Important insights about the formation mechanism and growth kinetics can be derived from *in situ* observations of structure formation. Using fluorescence polarization microscopy for *in situ* visualization of domain growth we observed that hexagonally ordered domains are preceded by the formation of an intermediately ordered

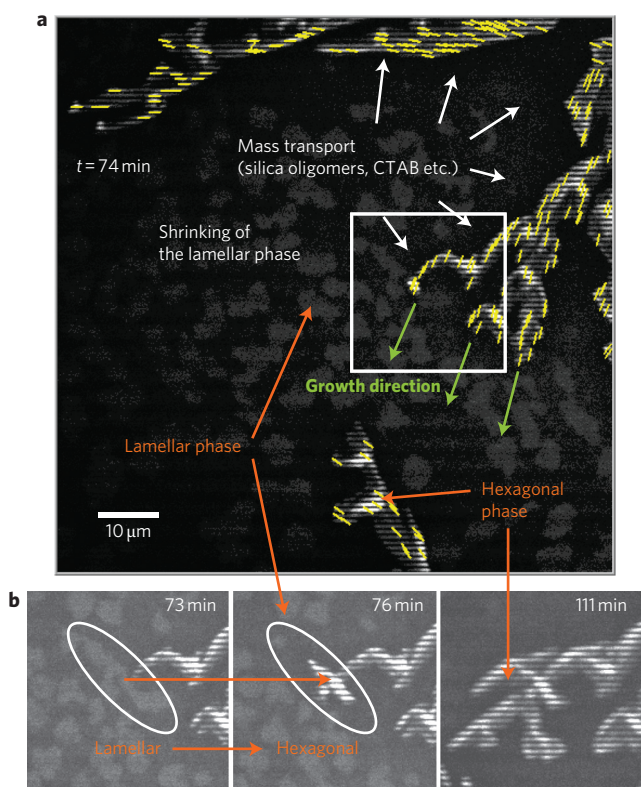


Figure 2 | Growth dynamics visualized by fluorescence microscopy.

a, Polarization-modulated confocal image extracted from Supplementary Movie S1 at $t = 74$ min showing two different structures: unpolarized lamellar structures (TDI shows homogeneous fluorescence patterns) and highly oriented hexagonal mesoporous layers (striped fluorescence patterns). The yellow stripes indicate the orientations of the pores at arbitrary positions. **b**, Frames extracted from Supplementary Movie S1 at 73, 76 and 111 min, respectively. The transition from a lamellar phase (homogeneous fluorescence pattern) to a hexagonal phase (striped fluorescence pattern) upon direct contact can be observed in the region marked with white ellipses.

(Supplementary Movie S1; Fig. 2). Although the hexagonally ordered domains appear as bright striped lines, this intermediate structure exhibits a homogeneous fluorescence polarization pattern. The homogeneous pattern indicates that the TDI molecules are randomly oriented within the intermediate structure, in contrast to the hexagonal phase, in which the fluorophores are aligned along the channels. During growth, this intermediate structure is not stable, and we observe that different discrete levels of fluorescence intensity appear (and disappear) successively, indicating the formation and disappearance of new layers of this ordered metastable phase (Supplementary Fig. S5 and Movie S2). Moreover, the diffusion coefficient of TDI molecules within this structure is orders of magnitude higher than that within the hexagonal phase or on the surface of the mesoporous film (Supplementary Fig. S6 and Movie S3). Interestingly, the observed TDI diffusion is very similar to that in a lamellar phase of pure CTAB in both cases: the single TDI molecules exhibit a totally random movement with similar diffusion coefficients (Supplementary Fig. S6 and Movie S3). There is therefore strong evidence that the observed intermediate structure is indeed a lamellar phase, which is metastable under our experimental conditions.

Strong growth dynamics can be observed for the lamellar and hexagonal structures. At first, numerous lamellar islands appear and increase continuously in size (Fig. 2). Two different mechanisms for the growth of the hexagonal layers are then observed.

The first shows rapid conversion of lamellar arrangements to hexagonal structures through a ‘seeding’ process. This occurs whenever a lamellar area is touched by the growing hexagonally ordered layers. The shape of the hexagonal structure created by this phase transition approximately follows the former lamellar area.

The second mechanism is deduced from the observation that the lamellar structures present in the vicinity of growing hexagonal domains successively vanish as the hexagonal domains expand (Fig. 2a,b). This process is comparable to Ostwald ripening, but here the growth of the hexagonal domains proceeds at the cost of the smaller lamellar structures. During this mechanism, mass transport of reactive molecules mediates growth towards the self-assembling hexagonal layers. The growth of each hexagonal domain is clearly anisotropic, and the determined orientations of the channels correspond to the main direction of the anisotropic growth. The hexagonal layers therefore grow preferentially in the direction of the nanochannels.

The process of domain growth can also be directly visualized at the single molecule level (Supplementary Movie S4). Before encapsulation of TDI molecules into the hexagonal phase, a random movement on the surface of the mesoporous film substrate is observed. As the hexagonal domain grows, the freely diffusing TDI molecules are successively encapsulated in the domain and, as a result, move slowly up and down the straight channels that have formed around them.

Next, we show how this *in situ* observation technique can be used to control domain growth. By recording sequences of topographic AFM images, the self-assembly process is visualized in real time (Supplementary Movie S5), and growth kinetics can therefore be quantified (Supplementary Figs S7,S8). As determined previously, the relative humidity is extremely important for domain growth¹⁹. Below a relative humidity of 30%, no domain formation was observed, probably because under these conditions the water concentration is too low to drive the hydrolysis reaction required for silicization (Supplementary Figs S3,S4 contain details and additional experimental evidence). In contrast, at relative humidities above 70%, the freshly formed domains degrade within tens of minutes (Supplementary Fig. S9). Under these conditions, the equilibrium of the hydrolysis reaction prevents stable structure formation. Using *in situ* observation of domain growth we determine the optimal relative humidity for the formation of large domains (~50%). Furthermore, by varying the temperature we were able to control the growth kinetics (Fig. 3). Lamellar-to-hexagonal transitions can be induced within seconds by rapidly lowering the temperature from 35 °C to room temperature, leading to small domain sizes of the order of 300 nm (our lateral resolution, see Fig. 3a). These domain sizes are very similar to typical domain sizes obtained using spin-coating (Supplementary Fig. S10). If the mesoporous film substrate is exposed to a constant temperature of 35 °C, one observes the formations of large domains on the scale of micrometres. Here, growth occurs on a timescale of minutes (Fig. 3b). In contrast, if the temperature is lowered to 25 °C, domain growth is slowed to hours. As a result, at this temperature, ultralarge domains are obtained that are close to a millimetre in size (Fig. 3c). In other words, slow kinetics lead to large domain sizes. We calculated that when going from seconds to minutes and hours, the domain areas increase typically by a factor of 10,000 and 1,000,000, respectively. Multiple factors contribute to this effect. First, slow growth leads to a reduction in the number of defects and thus to larger domains. Second, with temperature (and relative humidity) we can adjust the rate of delivery of reactive material from the reservoir to the surface (see sketch in Fig. 1a, left panel), thus changing growth kinetics and, ultimately, domain size. In addition, our approach of using a mesoporous film substrate offers additional versatile means through which to control domain

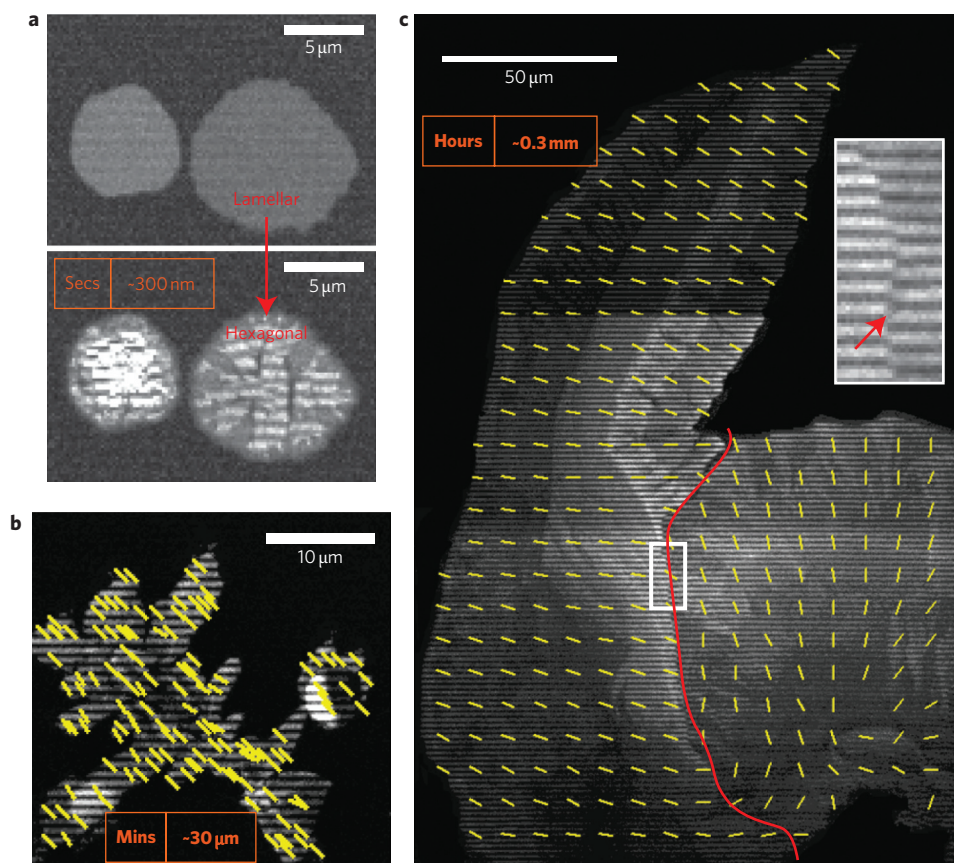


Figure 3 | Control of domain size. **a**, Fast domain formation (within seconds) leading to relatively small domain sizes. The lamellar-to-hexagonal transitions were induced by abrupt lowering of the temperature. **b**, Micrometre-sized hexagonal domain grown within tens of minutes at 35 °C exhibits a domain size in the range of 30 μm. Yellow bars correspond to the orientation of the channel system. **c**, Ultralarge highly structured domains with domain sizes of the order of 0.3 mm were obtained after several hours at room temperature. Inset: magnification of the region highlighted with a white square in which the boundary between the two domains can be visualized by the phase shift of the domains' polarization-modulated patterns, revealing different orientations of the channel systems (red arrow).

growth: the release of material can be tuned by choosing different pore sizes as well as by functionalization of the walls of the silica nanochannels²⁶.

The following picture therefore emerges. CTAB, TDI, water and silica oligomers are delivered onto the surface of the mesoporous film substrate, which acts as a reservoir for the formation of the hexagonal layers. Transient lamellar structures appear on the surface of the mesoporous film substrate. They exhibit strong dynamical changes in size as well as in height through expansion and the creation of new lamellas. A phase transition then occurs from the metastable lamellar layers to hexagonal bi- or multilayers, which are thermodynamically favoured due to the local composition of the constituents. This is followed by lateral growth of the hexagonal layers. Two growth mechanisms can be distinguished. In the first, direct contact between lamellar and hexagonal structures seeds a rapid phase transition to a hexagonal phase. The second process involves mass transport from the mesoporous film substrate surface towards the self-assembling hexagonal layers. The growth is anisotropic with a preferential direction along the channels. During the whole process, condensation of the silica oligomers occurs progressively and constitutes the driving force for the formation of the mesoporous layers (see Supplementary Figs S3, S4 for details and additional experimental evidence). Domain growth depends critically on the experimental conditions. Conditions that slow down domain growth result in ultralarge domain sizes with dimensions extending into the millimetre range, whereas the rapid formation of domains during spin-coating or a temperature

quench results in the formation of small domains. By adapting the temperature and relative humidity one can fine-tune the delivery rate of the molecular species out of the molecular sieve used as a reservoir. As a consequence, the growth rate and ultimately the domain size can be controlled, in addition to the healing of defects. After a typical aging time of several hours, polymerization of the silica matrix is complete, resulting in a stable hexagonal silica structure. Thus, the *in situ* visualization of the domain growth of silica mesoporous layers using AFM and fluorescence microscopy gives important insight into the mechanistic details of this self-assembly process, allowing domain growth to be controlled, and leading to ultralarge domains not achievable previously. In the future, the presented approach could be combined with existing structure-directing methodologies^{20,27,28} to additionally control the orientation of the individual domains.

Methods

Synthesis of the mesoporous film substrate. Hexagonal silica films were synthesized by means of evaporation-induced self-assembly (EISA)¹⁵. Samples were prepared by spin-coating precursor solutions onto cleaned glass coverslips. For the preparation of precursor solutions, 10 mmol (2.08 g) of tetraethoxysilane in 534 mmol (7.9 g) ethanol were prehydrolysed at 60 °C for 1 h under acidic catalysis (using 3 g of 0.2 M hydrochloric acid and 1.8 g of water). CTAB (2.00 mmol, 638 mg), the structure-directing agent, was added in 1,068 mmol (15.8 g) ethanol. Terrylene diimide (TDI), a very bright and photostable dye (structure shown in Fig. 1a, right panel)^{25,29}, was added to the solution at a concentration of $C = 1 \times 10^{-7} \text{ mol l}^{-1}$ for polarization-modulated confocal measurements, or at ultralow concentration ($C = 1 \times 10^{-10} \text{ mol l}^{-1}$) for single molecule investigations. This precursor solution was then spin-coated onto cleaned coverslips

(30 s at 3,000 r.p.m.), resulting in structured silica films with a thickness of ~120 nm (determined by ellipsometry).

Initiation of the growth of ultralarge domains of thin mesoporous layers. Silica condensation occurs within days following the formation of the mesoporous film substrate. As the degree of silica condensation influences the supply rate of the reactants it is important to control the aging time. In this study, domain growth on top of the mesoporous film substrate was always initiated after an aging time of 24 h at room temperature and relative humidity of 40–50%, as this aging time was optimal for the formation of large domain structures with a sufficient supply rate of the reactants onto the substrate surface. Domain growth was induced by varying the temperature and/or relative humidity, as explained in the main text.

Synthesis of hexagonal and lamellar phases of pure CTAB. For the hexagonal phase, 0.035 mmol (12.76 mg) of CTAB was dissolved in 223 mmol (4.01 g) deionized UV-radiated water. The solution was subsequently held in an ultrasonic bath for 15 s. TDI was added at a concentration of 1×10^{-7} mol l⁻¹ for ensemble fluorescence experiments and 1×10^{-10} mol l⁻¹ for single molecule experiments. A volume of 100 µl of solution was then spin-coated on a cleaned coverslip (45 s at 1,500 r.p.m.). Relative humidity was set at 50–60% during the spin-coating process. The samples were subsequently exposed to ethanol vapour for 1 h to complete the formation of the hexagonal structure. With this procedure, hexagonally structured thin films with a thickness of 15–20 nm were obtained (measured by AFM).

To obtain a lamellar phase of pure CTAB, 638 mg CTAB was dissolved in 23.7 g ethanol. Hydrochloric acid (3 g of 0.2 M) and 1.8 g of water were then added. TDI was then added at an ultralow concentration ($C = 1 \times 10^{-10}$ mol l⁻¹) for the single molecule experiments. A volume of 80 µl of solution was then spin-coated on a cleaned coverslip (30 s at 3,000 r.p.m.). The resulting films exhibited a lamellar structure, as determined by X-ray diffractometry (data not shown).

AFM imaging. The atomic force microscope used in all experiments was an Asylum Research MFP3D. Olympus AC160TS tapping-mode cantilevers ($f_{res} \approx 300$ kHz) were used with a free amplitude of 1 V and a setpoint of 0.85 V. The sample coverslips were immobilized with a small droplet of immersion oil on cover glasses that were fixed to the x - y stage by magnets. For measurements with temperature control, the samples were placed in an Asylum Research Bioheater. Relative humidity was kept constant with saturated solutions of various salts, depending on the relative humidity desired.

Polarization-modulated confocal microscopy. For orientation measurements the mesoporous films were investigated with a modified inverted confocal laser scanning microscope (ZEISS LSM 410). The experimental setup is schematically depicted in Supplementary Fig. S2a. An oil immersion objective with a high numerical aperture (ZEISS 63 × 1.4 oil) and a 633 nm He–Ne laser were used for excitation of the TDI dye molecules. The fluorescence light was separated from the laser light using a combination of filters consisting of a dichroic mirror (Q640LP AHF, Analysentechnik) and a fluorescence filter (HQ720/150 AHF, Analysentechnik). The fluorescence was detected with a photomultiplier. For the measurement of molecular orientation, a rotating $\lambda/2$ plate, placed just before the objective, was used to modulate the polarization plane of the excitation light. The fluorescence intensity of the dyes was recorded in dependence on the polarization angle of the excitation light. The scanning time was 128 ms per line, and the excitation modulation period was ~600 ms per rotation. During all measurements, the temperature was set using a temperature controller (Temp Control 37-2 digital, ZEISS), and the relative humidity was kept constant with saturated solutions of various salts, depending on the desired value of relative humidity.

The two-dimensional orientation of the molecules in the focal plane was determined using a custom Labview program by fitting a cosine-squared function to the data from a region of interest measuring 15 × 15 pixels centred at arbitrary positions according to the following equation:

$$I = A_0 \cos^2(\omega t - \Phi_{ref} + \Phi_{mol}) \quad (1)$$

where A_0 is the amplitude of the cosine-squared curve, ω is the angular rotation velocity of the $\lambda/2$ plate, Φ_{ref} is the phase of the modulated transmission signal, and Φ_{mol} is the in-plane angle of the TDI molecules. The zero value for the angle is given by the direction of the main axis of the polarizer, which corresponds here to the horizontal line in the confocal fluorescence images.

The transmission signal was used as reference to obtain the absolute angle of the transition dipole moment. It passed through a polarizer and was recorded simultaneously with the fluorescence signal. The sum of the pixel intensity values of the horizontal lines of the region of interest was plotted versus time, and was fitted with

$$I = A_1 \cos^2(\omega t - \Phi_{ref}) \quad (2)$$

where A_1 is the amplitude of the cosine-squared function, ω is the angular speed of the $\lambda/2$ plate, and Φ_{ref} is the phase of the signal. The accuracy for the determination of the angles was typically about $\pm 5^\circ$.

Wide-field microscopy and single particle tracking (SPT). The pathways of the single TDI dye molecules inside the hexagonal domains were monitored using a wide-field setup to investigate their diffusional behaviour. The setup consists of a Nikon Eclipse TE200 epifluorescence microscope with an oil-immersion objective of high numerical aperture (Nikon Plan Apo ×100/1.40 NA oil). The TDI dye molecules were excited at 633 nm with a He–Ne gas laser (Coherent) with an intensity of 0.3 kW cm⁻². Fluorescence was detected with an Andor iXon DV897 back-illuminated electron multiplying-charge-coupled device (EM-CCD) camera in frame transfer mode (512 × 512 pixels). Incident laser light was blocked by a dichroic mirror (640 nm cutoff, AHF) and a band-pass filter (730/140, AHF). Image series were recorded with a typical length between 300 and 600 frames and a time resolution of 400–1,000 ms per frame. The single TDI molecules appear as bright, diffraction-limited Gaussian-shaped patterns. Single particle tracking was used to determine the position of the molecules using a custom Labview program. The positioning accuracy was typically of the order of ± 5 nm.

Received 1 June 2010; accepted 19 November 2010;
published online 9 January 2011

References

- Davis, M. E. Ordered porous materials for emerging applications. *Nature* **417**, 813–821 (2002).
- Grosso, D. et al. Periodically ordered nanoscale islands and mesoporous films composed of nanocrystalline multimetallic oxides. *Nature Mater.* **3**, 787–792 (2004).
- Riehemann, K. et al. Nanomedicine—challenge and perspectives. *Angew. Chem. Int. Ed.* **48**, 872–897 (2009).
- Dag, Ö., Ozin, G. A., Yang, H., Reber, C. & Bussi ere, G. Photoluminescent silicon clusters in oriented hexagonal mesoporous silica film. *Adv. Mater.* **11**, 474–480 (1999).
- Sanchez, C., Boissiere, C., Grosso, D., Laberty, C. & Nicole, L. Design, synthesis, and properties of inorganic and hybrid thin films having periodically organized nanoporosity. *Chem. Mater.* **20**, 682–737 (2008).
- Yang, C. M., Cho, A. T., Pan, F. M., Tsai, T. G. & Chao, K. J. Spin-on mesoporous silica films with ultralow dielectric constants, ordered pore structures, and hydrophobic surfaces. *Adv. Mater.* **13**, 1099–1102 (2001).
- Chen, Z. et al. DNA translocation through an array of kinked nanopores. *Nature Mater.* **9**, 667–675 (2010).
- Grosso, D. et al. Two-dimensional hexagonal mesoporous silica thin films prepared from block copolymers: detailed characterization and formation mechanism. *Chem. Mater.* **13**, 1848–1856 (2001).
- Grosso, D. et al. Fundamentals of mesostructuring through evaporation-induced self-assembly. *Adv. Funct. Mater.* **14**, 309–322 (2004).
- Antonietti, M. & Ozin, G. A. Promises and problems of mesoscale materials chemistry or why meso? *Chem. Eur. J.* **10**, 28–41 (2004).
- Gibaud, A. et al. Evaporation-controlled self-assembly of silica surfactant mesophases. *J. Phys. Chem. B* **107**, 6114–6118 (2003).
- Doshi, D. A. et al. Peering into the self-assembly of surfactant templated thin-film silica mesophases. *J. Am. Chem. Soc.* **125**, 11646–11655 (2003).
- Lu, Y. F. et al. Continuous formation of supported cubic and hexagonal mesoporous films by sol gel dip-coating. *Nature* **389**, 364–368 (1997).
- Yang, H., Kuperman, A., Coombs, N., MamicheAfara, S. & Ozin, G. A. Synthesis of oriented films of mesoporous silica on mica. *Nature* **379**, 703–705 (1996).
- Brinker, C. J., Lu, Y. F., Sellinger, A. & Fan, H. Y. Evaporation-induced self-assembly: nanostructures made easy. *Adv. Mater.* **11**, 579–585 (1999).
- Kirstein, J. et al. Exploration of nanostructured channel systems with single-molecule probes. *Nature Mater.* **6**, 303–310 (2007).
- Z urner, A., Kirstein, J., D oblinger, M., Br auchle, C. & Bein, T. Visualizing single-molecule diffusion in mesoporous materials. *Nature* **450**, 705–708 (2007).
- Jung, C., Hellriegel, C., Michaelis, J. & Br auchle, C. Single-molecule traffic in mesoporous materials: translational, orientational, and spectral dynamics. *Adv. Mater.* **19**, 956–959 (2007).
- Jung, C. et al. Diffusion of oriented single molecules with switchable mobility in networks of long unidimensional nanochannels. *J. Am. Chem. Soc.* **130**, 1638–1648 (2008).
- Tolbert, S. H., Firouzi, A., Stucky, G. D. & Chmelka, B. F. Magnetic field alignment of ordered silicate-surfactant composites and mesoporous silica. *Science* **278**, 264–268 (1997).
- Platschek, B., Petkov, N. & Bein, T. Tuning the structure and orientation of hexagonally ordered mesoporous channels in anodic alumina membrane hosts: a 2D small-angle X-ray scattering study. *Angew. Chem. Int. Ed.* **45**, 1134–1138 (2006).
- Koganti, V. R. et al. Generalized coating route to silica and titania films with orthogonally tilted cylindrical nanopore arrays. *Nano Lett.* **6**, 2567–2570 (2006).

23. Yamauchi, Y. *et al.* Magnetically induced orientation of mesochannels in 2D-hexagonal mesoporous silica films. *J. Mater. Chem.* **16**, 3693–3700 (2006).
24. Schirmeisen, A., Anczykowski, B. & Fuchs, H. in *Nanotribology and Nanomechanics—An Introduction* (ed. Bushan, B.) (Springer, 2005).
25. Holtrup, F. O. *et al.* Terrylenimides: new NIR fluorescent dyes. *Eur. J. Chem. A* **3**, 219–225 (1997).
26. Lebold, T. *et al.* Tuning single-molecule dynamics in functionalized mesoporous silica. *Eur. J. Chem. A* **15**, 1661–1672 (2009).
27. Pang, J. *et al.* Directed aerosol writing of ordered silica nanostructures on arbitrary surfaces with self-assembling inks. *Small* **4**, 982–989 (2008).
28. Trau, M. *et al.* Microscopic patterning of orientated mesoscopic silica through guided growth. *Nature* **390**, 674–676 (1997).
29. Jung, C. *et al.* A new photostable terrylene diimide dye for applications in single molecule studies and membrane labeling. *J. Am. Chem. Soc.* **128**, 5283–5291 (2006).

Acknowledgements

The authors thank K. Müllen (Max Planck Institut) for kindly providing the TDI dye molecule, as well as T. Bein (LMU) for helpful discussions. This work was funded by SFB 486, SFB 749 and the Nanosystems Initiative Munich (NIM).

Author contributions

C.J. conceived, designed and performed the experiments, analysed the data and co-wrote the paper. P.S. and M.D. designed and performed the experiments, and analysed the data. R.K. conceived the experiments. J.M. and C.B. conceived the experiments and co-wrote the paper.

Additional information

The authors declare no competing financial interests. Supplementary information accompanies this paper at www.nature.com/naturenanotechnology. Reprints and permission information is available online at <http://npg.nature.com/reprintsandpermissions/>. Correspondence and requests for materials should be addressed to J.M. and C.B.